# Comfort-based floor design employing tuned inerter mass system

Qingjun Chen[a,b], Zhipeng Zhao[a,b], Yuying Xia[c], Chao Pan[d], Hao Luo[a], Ruifu Zhang[a,*]

[a] *Department of Disaster Mitigation for Structures, Tongji University, Shanghai 200092, China.*

[b] *State Key Laboratory of Disaster Reduction in Civil Engineering, Tongji University, Shanghai 200092, China.*

[c] S*wansea University, College of Engineering, Fabian Way, SA1 8EN, Swansea, UK*

[d] *College of Civil Engineering, Yantai University, Yantai 264005, China.*

**Abstract**

A comfort-based optimal method has been developed for designing floors using tuned inerter mass systems (TIMS) to reduce the vertical-vibration response of floors subjected to human-induced excitations. Acceleration response of the floor and output force of TIMS were first derived via stochastic analysis. Subsequently, variation patterns in acceleration-response and output-force ratios were studied and compared by changing values of TIMS parameters. Based on the results of this parametric investigation, a comfort-based optimal design method and the corresponding procedure to be followed were developed. In the proposed method, the weighted average of the required additional tuned mass and TIMS output force are expected to be minimized whilst realizing the expected level of satisfaction in terms of target comfort performance of the floor structure (i.e., target acceleration response ratio). For different design targets, optimized TIMS parameters can be obtained using the proposed design method, and such design cases have been demonstrated by performing time-history analysis under different external human-induced excitations. Results of the said analysis demonstrate that the proposed design method effectively satisfies comfort-performance objectives of a floor with optimal actual mass through use of an inerter system. In addition, the proposed method can be used to maintain a balance between the control cost, additional tuned mass, and structural comfort performance.

**Keywords:** inerter; human-induced excitation; comfort-based design; floor vibration.

## 1 Introduction

Structural control has been proven to be an effective means for mitigating dynamic responses of structures subjected to different types of excitations [1-3]. Many researches have been performed to propose various strategies for reducing the unrecoverable damage caused by natural phenomena, such as earthquakes, as well as satisfying the desired level of comfort from structures [4-7]. In practical applications, excessive floor-vibration responses of spatial structures and large-span bridges owing to human-induced excitations lead to structural insecurity and physical discomfort [8-10]. This problem is becoming increasingly common with the growing use of high-strength materials, low-stiffness supporting

* Corresponding author.

E-mail address: zhangruifu@tongji.edu.cn (R. F. Zhang)

components, and large-span structures. Resonance may occur when the walking frequency of humans approaches a value close to the natural frequency of the floor structure. In accordance with an extant study on floor vibration [11], this phenomenon is induced by the low stiffness and damping of floor structures. To control the excessive vibration of floor structures, several optional approaches can be adopted for structural design [4, 12, 13]. Commonly adopted methods include the use of components with higher stiffness, viscous damping, tuned mass dampers (TMDs). TMDs [14-16] can be set within floor structures with a view to attenuate the inherent vibration response. A typical TMD comprises a mass element, damping element, and spring element; it is attached to the floor structure and absorbs floor vibration energy by tuning the frequency of the floor structure. TMDs represent a type of vibration mitigating system that operates over a narrow frequency range and is effective in controlling floor vibrations due to human-induced excitations. For a footbridge system equipped with vertical and lateral TMDs, Elsa et al. [17] discussed the design strategy and effectiveness evaluation on the basis of experimental investigations. With the main objective of satisfying comfort requirements under human-induced vibrations, Tubino [15] developed an optimal design method for TMDs along with a specific optimization criterion. To determine the robustness of TMDs, Lievens et al. [18] proposed a robust optimization approach, wherein uncertainties associated with changes in environmental conditions and vibration-reduction measures were considered.

Generally, however, the actual mass of the mass element in traditional TMDs is large, and sometimes, it is difficult to install such a TMD within floor structures. This difficulty can be overcome by adding an inerter element incorporated within the TMD to reduce the weight of a conventional TMD. An inerter is a device comprising two terminals that can move freely to provide a resisting force proportional to their relative acceleration, and based on the principle of the two-terminal mass element, a small actual mass can be magnified into a large apparent mass [19-21]. At the end of the last century, to amplify viscous-damping forces, Arakaki et al. [22] used the ball screw mechanism to transform linear motion into high-speed rotation by vicariously utilizing the inerter mechanism. Around the same time, the concept of the inerter was introduced in the field of mechanical control by Smith [23], who developed inerter equipment using gear-system devices. Unlike the traditional one-terminal mass element, an inerter is a two-terminal mass element, wherein the applied force is proportional to the relative acceleration of the terminals (Fig. 1). This force can be expressed as follows.

$$F_I = m_{in}\left(\ddot{u}_2 - \ddot{u}_1\right), \tag{1}$$

where $F_I$ denotes the axial force of the inerter, which is opposite to the external force in equilibrium; $m_{in}$ denotes the inertance; and $\ddot{u}_1$ and $\ddot{u}_2$ denote acceleration values at the two inerter terminals.

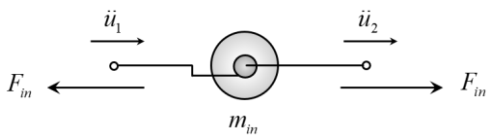


Fig. 1. Schematic of two-terminal inerter element.

Different implementation mechanisms have been proposed for the inerter system, such as the rack-and-pinion [23], ball screw [24, 25], electromagnetic [26], and hydraulic [27] mechanisms. In the inerter system, the inerter, damping, and spring elements are used as the energy absorbing, energy-dissipation, and frequency-tuned devices, respectively. To illustrate the basic design theory of a structure equipped with an inerter system, Ikago et al. [28] proposed a simple design method for a single degree of freedom (SDOF) structure equipped with an inerter system. They performed shake table tests for a small-scale inerter system to verify the effectiveness of their proposed design method. Pan et al. [29] proposed an optimal design method for the inerter system that satisfied the performance and cost-control demands of the end application. Later, the close-form solutions of Root-Mean-Square (RMS) responses of structure with the three inerter systems were derived theoretically by Pan and Zhang [6]. Based on the derived solutions, they further proposed a performance-demand-based practical design approach for the three classic inerter systems in the extreme response condition. The mentioned optimal design methods were basically developed for the condition of the structure equipped with classic inerter system under the seismic excitation, which cannot be directly applied for the comfort-based issue.

The concept of the inerter has been used in different areas of civil engineering [28, 30-32]. A type of electromagnetic inertial mass damper comprising a ball screw in combination with a rotating inertial mass was developed to control vibrations of structures subjected to earthquakes [33]. The effectiveness of the inerter system in controlling the response of rigid superstructures was confirmed by Wang et al. [34]. A seismically excited system equipped with an inerter damper for vibration isolation of primary SDOF and two-degree-of-freedom structures was studied by Lazar et al. [35]. Further, the seismic response of a tank was controlled by an inerter system used in combination with a hybrid control method [30, 36].

For greater reduction in dynamic response, the concept of tuning was used to integrate an inerter element into conventional TMD configurations [2, 37-39]. For base-isolated structure, De Domenico and Ricciardi [32, 40] proposed the optimal design of inerter-based TMD systems within a stochastic framework, and Hashimoto et al. [41] compared different types of inerter-based structural control layouts with the inerter installed in different configurations and positions. Pietrosanti et al. [42] proposed the optimal design method of the inerter-based TMD system for base-fixed structure by following three different design methodologies. However, in the layout suggested by their design approach, the inerter element was mounted between the tuned mass and ground, which is not suitable for vibration control of the floor structure, since the control device must be directly fixed on the floor structure. One type of TMD including a special inerter was proposed by fixing the inerter element between the tuned mass and adjacent floor, and this damper was proven to possess a broad spectrum of applicability [43]. To verify the effectiveness of such a system, an experiment was performed [44]. Compared to conventional TMDs, the tuned mass required in the tuned inerter mass system (TIMS) was reduced effectively through the use of an inerter element. It was also demonstrated that the use of the inerter improved the performance of the system when compared to TMD systems with comparable effective mass (including both inertance $m_{in}$ and tuned mass $m_t$) [32, 40]. Similarly, a skyhook semi-active inerter configuration was analyzed for comfort-based optimal design using different control laws [19].

Extant researches have mainly focused on developing different kinds of TMDs in combination with inerters, but the design method and potential use of TMDs have not received sufficient attention. Comfort-based utilization of TMDs equipped with inerters to inhibit floor vibrations produced by human-induced excitations still has potential research value, especially in terms of design methodologies. The greatest advantage of a TMD–inerter combination is that a small actual mass is used in the control system of the floor compared to that used in conventional TMDs. To more effectively mitigate floor vibrations due to human-induced excitation and alleviate installation problems through use of a small actual mass, a TMD–inerter combination was used in this study (Fig. 2). This simplified model of the floor structure [11, 15, 45] is widely used for the design and analysis of mitigation of floor vibration due to human-induced excitation. In the proposed TIMS design, a tuned mass $m_t$ was connected to the floor structure via spring element $k_d$ and damping element $c_d$. A viscous- or eddy-current-damping element can be used as the energy-dissipation element in TIMS. The inerter element with apparent mass $m_{in}$ was placed between the tuned mass element and floor structure.

Based on the target comfort performance level and control cost factor, a comfort-based optimal design method has been developed designing TIMS-equipped floor structures to reduce vertical vibration responses of floors subjected to human-induced excitations. Equations of motion of a TIMS-equipped floor structure were established. Using random analysis, solutions of stochastic responses were obtained. Subsequently, expressions for optimization indicators, namely, the comfort performance indicator $\gamma_A$, control cost indicator $\gamma_{F_d}$, and tuned mass ratio $\mu_t$, were derived. Next, a series of floor structures equipped with TIMS were designed in accordance with different comfort requirements through use of the proposed method. To verify the effectiveness of the proposed design method, several design cases were examined via time-domain analysis.

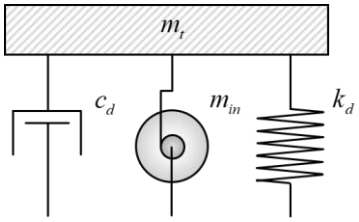


Fig. 2. Mechanical diagram of TIMS.

## 2 Theoretical analysis of floor equipped with TIMS

### 2.1 Mechanical model

A floor structure subject to human-induced excitations can be transformed into a single-degree-of-freedom (SDOF) structure for dynamic analysis. To evaluate the vibration control efficiency of TIMS with regard to SDOF system [11, 15, 45], a calculation model of the floor structure equipped with TIMS was established (Fig. 3). The floor structure was simplified to represent an SDOF system of mass $m$ attached to the supporting ground via spring and damping elements $k$ and $c$, respectively. Further, $x$ and $x_t$ denote displacements of the floor structure $m$ and TIMS tuned mass $m_t$,

respectively.

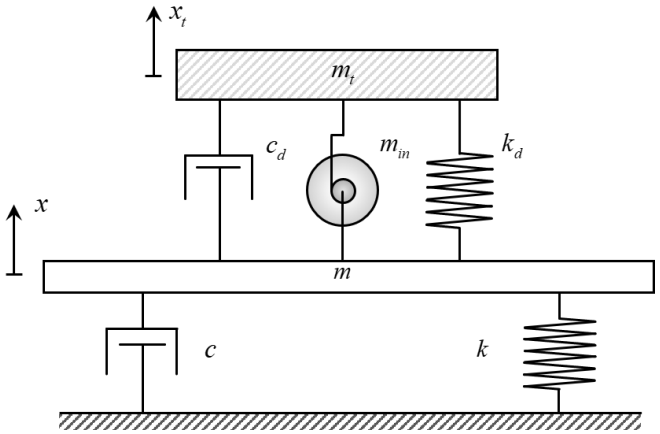

Fig. 3. Schematic of the floor structure with TIMS.

### 2.2 Governing equation of motion

The governing equation of motion for the system depicted in Fig. 3(b) can be expressed as

$$\begin{cases} m\ddot{x} + c\dot{x} + kx + m_{in}(\ddot{x} - \ddot{x}_t) + c_d(\dot{x} - \dot{x}_t) + k_d(x - x_t) = -F(t) \\ m_t\ddot{x}_t + m_{in}(\ddot{x}_t - \ddot{x}) - c_d(\dot{x} - \dot{x}_t) - k_d(x - x_t) = 0 \end{cases}, \tag{2}$$

wherein $\ddot{x}$ and $\dot{x}$ denote acceleration and velocity of the floor structure; $\ddot{x}_t$ and $\dot{x}_t$ denote acceleration and velocity of the tuned mass in TIMS; and $F(t)$ denotes the force of human-induced excitations.

The natural frequency $\omega_s$ and inherent damping ratio $\zeta$ of the floor structure can be determined using following relations.

$$\omega_s = \sqrt{\frac{k}{m}},\ \zeta = \frac{c}{2m\omega_s}. \tag{3}$$

To simplify the above governing equations, the dimensionless tuned mass ratio $\mu_t$, inerter-mass ratio $\mu_{in}$, stiffness ratio $\kappa$, nominal damping ratio $\xi$, and pedestrian weight ratio $\mu_p$ can be defined as follow.

$$\mu_t = \frac{m_t}{m},\ \mu_{in} = \frac{m_{in}}{m},\ \kappa = \frac{k_d}{k},\ \xi = \frac{c_d}{2\sqrt{mk}},\ \mu_p = \frac{m_p}{m}. \tag{4}$$

Subsequently, Eq. (2) can be rewritten as

$$\begin{cases} \ddot{x}(t) + 2\zeta\omega_s\dot{x}(t) + \omega_s^2 x(t) + \mu_{in}[\ddot{x}(t) - \ddot{x}_t(t)] + 2\xi\omega_s[\dot{x}(t) - \dot{x}_t(t)] + \omega_s^2\kappa[x(t) - x_t(t)] = -\mu_p a_h(t) \\ \mu_t\ddot{x}_t(t) + \mu_{in}[\ddot{x}_t(t) - \ddot{x}(t)] + 2\xi\omega_s[\dot{x}_t(t) - \dot{x}(t)] + \omega_s^2\kappa[x_t(t) - x(t)] = 0 \end{cases} \tag{5}$$

By using Newmark's algorithm [46], this equation can be solved to obtain numerical solutions for the controlled floor structure equipped with TIMS, i.e., the dynamic response of the floor structure subject to human-induced excitations.

### 2.3 Human-induced excitations

Resonance may occur when the natural frequency of the floor attains a value approximately equal to the frequency of daily human activities [47]. Human-induced excitations along the vertical direction can be expressed as follow [48], which is widely used for the simulation of human-induced excitation in the time domain,

$$F(t) = m_p g[1+\sum_{i=1}^{k}\alpha_i \sin(2i\pi ft-\phi_i)]=m_p a_h(t)\,, \tag{6}$$

where $F(t)$ denotes the human-induced excitation; $t$ denotes time; $m_p$ denotes weight of a single pedestrian; and $f$ denotes walking frequency. Further, $\alpha_i$ denotes the factor of the $i^{th}$ harmonic dynamic load; $\phi_i$ denotes the initial phase of the $i^{th}$ dynamic load; and $k$ represents harmonic load orders considered for the load. Lastly, $a_h(t)$ denotes the acceleration due to human-induced excitation.

Based on the theory of vibration-signal analysis, the human-induced-excitation model proposed by Bachmann and Ammann [49] was used in this study. Vertical harmonic loads of the first three orders were considered; subsequently, $\alpha_i$ and $\phi_i$ were determined using following relations.

$$\begin{aligned}&\alpha_1 = 0.4+0.25(f-2)\\ &\alpha_2=\alpha_3=0.1\\ &\phi_1=0,\ \phi_2=\phi_3=\pi/2\end{aligned}\quad . \tag{7}$$

The mass of a single pedestrian $m_p$ was assumed to be 70 kg, whereas the normal walking frequency of the pedestrian was considered to lie in the range of 1.8–2.5 Hz [48, 50]. As a representative example, a time-history curve of the human-induced excitation $a_h(t)$ at 2.2 Hz has been depicted in Fig. 4. For a given floor equipped with TMD and TIMS, its maximum response can be simulated under action of quasi-resonant vibrations, the frequency of which approximately equals that of the floor structure [15, 18, 48].

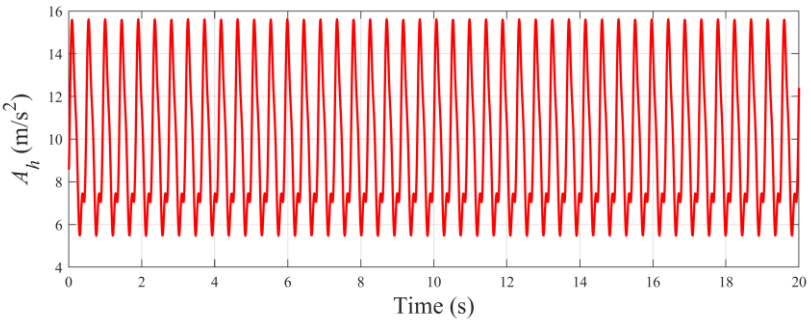


Fig. 4 Time history of typical human-induced excitation ( $f$ =2.2 Hz [50]) .

In the given frequency band of pedestrian walking motion, with the consideration of variations in walking frequencies, the human-induced excitations can be further considered as a random process, proposed by some researchers [15, 51]. Accordingly, the governing equation of motion for the system Eq. (4) will be solved as a random process as follow.

### 2.4 Stochastic solutions

If the human-induced excitation considered as a random process [15, 51], theories of random vibration will be employed to estimate the stochastic dynamic response of floor structures controlled via use of TIMS. Assuming the floor structure to be initially static (i.e., $x(0)=\dot{x}(0)=x_t(0)=\dot{x}_t(0)$) and the input excitation to represent harmonic motion with a circular frequency $\Omega$, Eq. (5) can be transformed into the Laplace domain as follows.

$$\begin{cases}[s^2(1+\mu_{in})+2\omega_s(\zeta+\xi)s+\omega_s^2(1+\kappa)]X(s)-[s^2\mu_{in}+2\xi\omega_s s+\omega_s^2\kappa]X_t(s)=-\mu_p A_h(s) \\ -[s^2\mu_{in}+2\xi\omega_s s+\omega_s^2\kappa]X(s)+[s^2(\mu_t+\mu_{in})+2\xi\omega_s s+\omega_s^2\kappa]X_t(s)=0\end{cases}, \tag{8}$$

wherein $s=\mathrm{i}\Omega$ ( i = imaginary number) and $X(s)$, $X_t(s)$, and $A_h(s)$ denote Laplace transforms of parameters $x(t)$, $x_t(t)$, and $a_h(t)$, respectively. Based on Eq. (8), displacement responses in terms of the floor structure and tuned masses $X(s)$ and $X_t(s)$ can easily be deduces as follows.

$$X(s)=-\frac{s^2(\mu_{in}+\mu_t)+2s\xi\omega_s+\kappa\omega_s^2}{D(\mu_{in},\mu_t,\kappa,\xi,\zeta,\omega_s)}\mu_p A_h(s), \tag{9}$$

$$X_t(s)=-\frac{s^2\mu_{in}+\omega_s(2s\xi+\kappa\omega_s)}{D(\mu_{in},\mu_t,\kappa,\xi,\zeta,\omega_s)}\mu_p A_h(s), \tag{10}$$

wherein

$$D(\mu_{in},\mu_t,\kappa,\xi,\zeta,\omega_s)=\begin{bmatrix}s^4(\mu_{in}+\mu_t+\mu_{in}\mu_t)+\kappa\omega_s^4+s^3(2\mu_{in}\zeta\omega_s+2\mu_t\zeta\omega_s+2\xi\omega_s+2\mu_t\xi\omega_s)\\+s^2(\kappa\omega_s^2+\mu_{in}\omega_s^2+\mu_t\omega_s^2+\kappa\mu_t\omega_s^2+4\zeta\xi\omega_s^2)+s(2\kappa\zeta\omega_s^3+2\xi\omega_s^3)\end{bmatrix}. \tag{11}$$

The transfer function between the Laplace transforms of floor structure's displacement $X(s)$ and human-induced excitation $A_h(s)$ can be expressed as follows.

$$H_A(\mathrm{i}\Omega)=\left.\frac{s^2X(s)}{\mu_p A_h(s)}\right|_{s=\mathrm{i}\Omega}. \tag{12}$$

This function describes the explicit relationship between the floor structure's acceleration response and external human-induced excitation. Comfort-control costs can be evaluated in accordance with the normalized TIMS output force $f_d(t)$ obtained from Eq. (5) as under.

$$f_d(t)=f_{d,k}(t)+f_{d,m}(t)+f_{d,c}(t)=\kappa\omega_s^2[x(t)-x_t(t)]+\mu_{in}[\ddot{x}(t)-\ddot{x}_t(t)]+2\xi\omega_s[\dot{x}(t)-\dot{x}_t(t)]. \tag{13}$$

As expressed in Eq. (13), normalized output forces $f_d$ are obtained from normalized spring force $f_{d,k}$ of $k_d$, normalized inertia force $f_{d,m}$ of $m_d$, and normalized damping force $f_{d,c}$ of $c_d$. Using the Laplace transform, the transfer function corresponding to the output force relative to the input provided by TIMS can be expressed as follows.

$$H_{F_d}(\mathrm{i}\Omega)=\left.\frac{(\kappa\omega_s^2+\mu_{in}s^2+2\xi\omega_s s)[X(s)-X_t(s)]}{\mu_p A_h(s)}\right|_{s=\mathrm{i}\Omega}. \tag{14}$$

Subsequently, the output power spectrum $S_Y(\Omega)$ of the system can be presented as follows.

$$S_Y(\Omega) = \left|H(\mathrm{i}\Omega)\right|^2 S_X(\Omega), \tag{15}$$

wherein $S_X(\Omega)$ denotes the input power spectrum and $H(\mathrm{i}\Omega)$ denotes the transfer function between the input variable $x$ and output variable $y$. To evaluate the total degree of dynamic response and comfort control costs, RMS of the output variable was chosen as the target function and expressed as

$$\sigma_Y = \sqrt{\int_{\beta_l}^{\beta_u} S_Y(\beta\omega_s)\omega_s \mathrm{d}\beta}, \tag{16}$$

wherein $\beta = \Omega/\omega_s$ denotes the circle frequency ratio and $\beta_l$ and $\beta_u$ denote the lower and upper bounds of the integration interval, respectively. Substituting Eq. (15) into Eq. (16), the RMS value can be rewritten as follows:

$$\sigma_Y = \sqrt{\int_{\beta_l}^{\beta_u} \left|H(\mathrm{i}\beta\omega_s)\right|^2 S_X(\beta\omega_s)\omega_s \mathrm{d}\beta}. \tag{17}$$

To calculate the value of $\sigma_Y$, the square moduli of transfer functions for $H_A(\mathrm{i}\beta\omega_s)$ and $H_{F_d}(\mathrm{i}\beta\omega_s)$ of the floor structure can explicitly be expressed as

$$\left|H_A(\mathrm{i}\beta\omega_s)\right|^2 = \frac{\beta^4\omega_s^2\left[4\beta^2\xi^2 + \left(\beta^2\mu_{in} + \beta^2\mu_t - \kappa\right)^2\right]}{E(\kappa, \mu_{in}, \mu_t, \xi, \zeta, \beta)}, \tag{18}$$

$$\left|H_{F_d}(\mathrm{i}\beta\omega_s)\right|^2 = \frac{\beta^4\mu_t^2\left[4\beta^2\xi^2 + \left(\kappa - \beta^2\mu_{in}\right)^2\right]}{E(\kappa, \mu_{in}, \mu_t, \xi, \zeta, \beta)}, \tag{19}$$

wherein

$$E(\kappa, \mu_{in}, \mu_t, \xi, \zeta, \beta) = \begin{bmatrix} 4\beta^2\left(\beta^2(\xi + \zeta\mu_{in} + (\zeta + \xi)\mu_t) - \zeta\kappa - \xi\right)^2 \\ +\left(\kappa - \beta^2\kappa - 4\beta^2\zeta\xi + \beta^2\left(\beta^2 - \kappa - 1\right)\mu_t + \beta^2\mu_{in}\left(\beta^2 + \beta^2\mu_t - 1\right)\right)^2 \end{bmatrix}. \tag{20}$$

Here, the RMS value $\sigma_A$ of acceleration responses of the floor structure equipped with TIMS and output force $\sigma_{F_d}$ under the human-induced excitation $S_{a_h}(\Omega)$ can be expressed as

$$\sigma_A = \sqrt{\int_{\beta_l}^{\beta_u} \left|H_A(\mathrm{i}\beta\omega_s)\right|^2 S_{a_h}(\beta\omega_s)\omega_s \mathrm{d}\beta}, \tag{21}$$

$$\sigma_{F_d} = \sqrt{\int_{\beta_l}^{\beta_u} \left|H_{F_d}(\mathrm{i}\beta\omega)\right|^2 S_{a_h}(\beta\omega_s)\omega_s \mathrm{d}\beta}, \tag{22}$$

where $\left|H_A(\mathrm{i}\beta\omega_s)\right|^2$ and $\left|H_{F_d}(\mathrm{i}\beta\omega_s)\right|^2$ can be calculated using Eqs. (18) and (19), respectively.

### 2.5 Evaluation indicators

Dimensionless indicators (i.e., the acceleration response ratio $\gamma_A$, output force ratio $\gamma_{F_d}$, and additional tuned mass ratio $\gamma_t$) to evaluate the dynamic performance of the floor structure and vibration-mitigation efficiency of TIMS can be defined as follows [48].

$$\gamma_A(\mu_t, \mu_{in}, \kappa, \xi) = \frac{\sigma_A}{\sigma_{A_u}} = \sqrt{\frac{\int_{\beta_l}^{\beta_u} \left|H_A(\mathrm{i}\beta\omega_s)\right|^2 S_{a_h}(\beta\omega_s)\omega_s \mathrm{d}\beta}{\int_{\beta_l}^{\beta_u} \left|H_{A_u}(\mathrm{i}\beta\omega_s)\right|^2 S_{a_h}(\beta\omega_s)\omega_s \mathrm{d}\beta}}, \tag{23}$$

$$\gamma_{F_d}\left(\mu_t,\mu_{in},\kappa,\xi\right)=\frac{\sigma_{F_d}}{\sigma_{F_{du}}}=\sqrt{\frac{\int_{\beta_l}^{\beta_u}\left|H_{F_d}\left(\mathrm{i}\beta\omega\right)\right|^2 S_{a_h}\left(\beta\omega_s\right)\omega_s\mathrm{d}\beta}{\int_{\beta_l}^{\beta_u}\left|H_{F_{du}}\left(\mathrm{i}\beta\omega\right)\right|^2 S_{a_h}\left(\beta\omega_s\right)\omega_s\mathrm{d}\beta}}\,, \tag{24}$$

$$\gamma_t\left(\mu_t\right)=\mu_t\,. \tag{25}$$

where $\gamma_A$ denotes ratio of the RMS acceleration response of the floor structure equipped with TIMS to that of the original floor structure; $\gamma_{F_d}$ denotes ratio of the RMS value TIMS output force to that of the resistance force of the original floor structure (provided by inherent damping and stiffness); and $\gamma_t$ equals $\mu_t$. Parameters $\sigma_{A_u}$ and $\sigma_{F_{du}}$, respectively, denote the RMS acceleration response and resistance force of the original floor structure. In addition, $\left|H_{A_u}\left(\mathrm{i}\beta\omega_s\right)\right|$ and $\left|H_{F_{du}}\left(\mathrm{i}\beta\omega_s\right)\right|$ denote corresponding transfer-function moduli expressed as follows.

$$\left|H_{A_u}\left(\mathrm{i}\beta\omega_s\right)\right|^2=\frac{\beta^4}{1+\beta^4+\beta^2\left(4\zeta^2-2\right)}\,, \tag{26}$$

$$\left|H_{F_{du}}\left(\mathrm{i}\beta\omega_s\right)\right|^2=\frac{1+4\beta^2\xi^2}{1+\beta^4+\beta^2\left(4\zeta^2-2\right)}\,. \tag{27}$$

Substituting Eqs. (26) and (27) into Eqs. (23) and (24), final expressions for $\gamma_A$ and $\gamma_{F_d}$ can be obtained. Considering the frequency range of human-induced excitations, integral operations for indicators $\gamma_A$ and $\gamma_{F_d}$ in Eqs. (23) and (24) were performed between lower and upper bounds $\beta_l$ and $\beta_u$, respectively, of human-induced excitations.

## 3 Optimal design of floor structure equipped with TIMS

### 3.1 Parametric study

As discussed in section 2.4, the comfort-performance state of the floor structure and inertia force of TIMS demonstrate a nonlinear correlation with TIMS parameters $\mu_t$, $\mu_{in}$, $\kappa$, and $\xi$. To analyze the vibration mitigation effect of TIMS and explore the impact of TIMS parameters on dynamic performance of the floor structure, a parametric analysis was performed in this study.

A floor structure with an inherent damping ratio $\zeta=2\%$ and mass $m=1000$ kg was established, and its natural frequency was chosen to be 2 Hz, thereby ensuring its consistency with that of the human-induced excitation and thus, satisfying the resonance requirement. Assuming the TIMS tuned mass ratio $\mu_t=0.10$ and inerter-mass ratio $\mu_m=0.05,\ 0.10,\ 0.20$, in successive cases, values of $\gamma_A$ and $\gamma_{F_d}$ were calculated using Eqs. (23) and (24) with variable nominal damping and stiffness ratios—$\xi$ and $\kappa$, respectively. Considering the existing variation of walking frequency, the human-induced excitation, which is usually narrow-band random processes, was simulated by the white noise [15, 51]. Fig. 5 and Fig. 6 depict contour plots of results obtained for $\gamma_A$ and $\gamma_{F_d}$, wherein values of $\xi$ and $\kappa$ are represented along the X- and Y-axis, respectively. Following observations can be made from the contour plots.

1) With regards to $\gamma_A$ corresponding to the floor structure equipped with TIMS, as depicted in Fig. 5, the minimum-value region (i.e., the cool-colored area) is located in the inner part of the contour curve. The topography of contour curve resembles that of a valley. With the increase in $\mu_{in}$, the bottom of valley (i.e., the minimum value of $\gamma_A$) shifts towards the upper-right corner of the curve, which indicates that a combination of large values of $\xi$ and $\kappa$ is more effective in dissipating the vibration energy and further suppressing the vibration level of the floor. Observed trends concerning variations in the values of $\gamma_A$, as depicted in Fig. 5 (a)–(c), are nearly identical, although specific values are different. The acceleration mitigation effect of TIMS is positively related to changes in the value of $\mu_{in}$. With regard to trends concerning values of $\gamma_{F_d}$, as depicted in Fig. 6, the maximum value of $\gamma_{F_d}$ can be realized as $\xi$ approaches its lower bound. As the value of $\mu_{in}$ increases, the location of maximum $\gamma_{F_d}$ moves upwards along the Y-axis. In this single-peaked mountain topography, the observed peak value and its corresponding location are positively related to TIMS design parameters, especially $\mu_{in}$.

2) A comparison of the different contours of $\gamma_A$ and $\gamma_{F_d}$ depicted in Fig. 5 and Fig. 6 indicates that observed variation trends for $\gamma_A$ and $\gamma_{F_d}$ are largely different. The location of minimum $\gamma_A$ is different from that of minimum $\gamma_{F_d}$. For sake of performance-oriented design, if the target performance (evaluated by $\gamma_A$) is preset, the points on the contour line of $\gamma_A$, the value of which is consistent with the target performance demand can satisfy the control requirement. However, among these points, TIMS output forces can assume values vastly different from each other. To facilitate an economic TIMS design, the optimal parameter set must be located at the critical point, corresponding to where the value of $\gamma_{F_d}$ is minimum. Such a point would also mark the intersection of the valley curve of $\gamma_A$ and peak line of $\gamma_{F_d}$. To determine this optimal parameter set, a solution to the nonlinear constraint problem is proposed in this study.

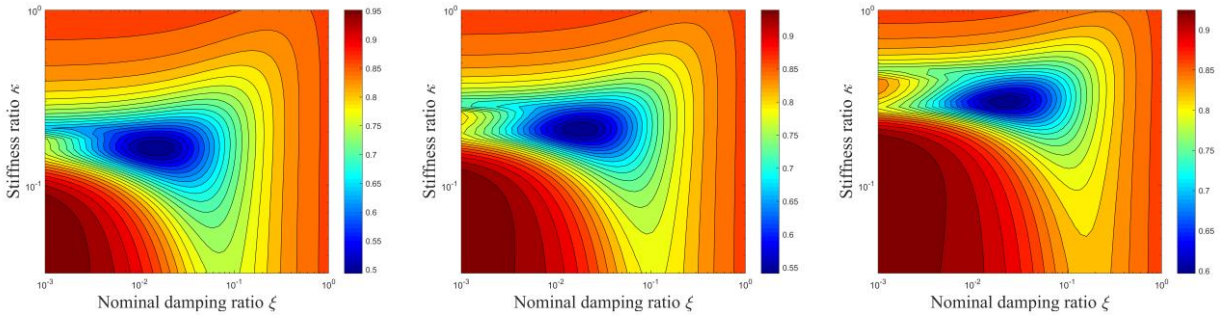


(a) (b) (c)

Fig. 5. Contour plots depicting variations in value of $\gamma_A$ corresponding to floor structure equipped with TIMS under human-induced excitation for $\kappa \in [0.05,\ 1.0]$, and $\xi \in [0.001,\ 1.0]$—(a) $\mu_{in} = 0.05$; (b) $\mu_{in} = 0.10$; and (c) $\mu_{in} = 0.20$.

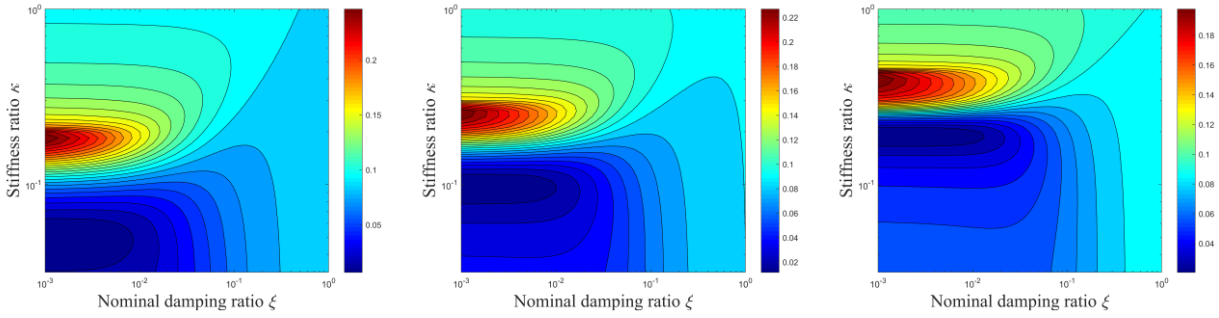


(a) (b) (c)

Fig. 6. Contour plots depicting variations in value of $\gamma_{F_d}$ corresponding to floor structure equipped with TIMS under human-induced excitation for $\kappa \in [0.05,\ 1.0]$, and $\xi \in [0.001,\ 1.0]$—(a) $\mu_{in} = 0.05$; (b) $\mu_{in} = 0.10$; and (c) $\mu_{in} = 0.20$.

### 3.2 Optimal design method

For a floor structure subjected to human-induced excitations, the acceleration response is always limited by the issue of comfort. From the practical engineering viewpoint [6, 29], it is better to minimize the cost of vibration mitigation along with the satisfaction of the performance level expected from the floor, thereby representing an economic solution. In addition, if the overall mass of the vibration-control system is large, it leads to difficulties associated with its installation and use. Considering the mass-enhancement effect of the inerter element in TIMS, overall mass of the vibration-control system can be reduced via use of an inerter element. This is an effective means to reduce the acceleration response with a relatively small tuned mass. This is the essential difference between TIMS and other control systems. In other words, a satisfactory design represents a trade-off between the dynamic performance level of the floor, overall mass of the vibration-control system, and corresponding control cost. The similar numerical approach for optimization has been successfully used by the same authors for the design of structures with inerter systems for the mitigation of seismic responses [6, 29].

For the floor structure equipped with TIMS, the above comfort issue can be represented in the form of the floor's acceleration (i.e., acceleration response ratio $\gamma_A$ in Eq. (23)); control cost can be reflected by the output force ratio $\gamma_{F_d}$; and value of $m_t$ can represented by the additional tuned mass ratio $\gamma_t$. Using the integration operation expressed in Eq. (23) and (24), the total response over the specified frequency domain of human-induced excitations can be considered. The optimal design problem can, therefore, be formulated as follows.

$$\begin{aligned} \underset{\mathbf{x}}{\text{minimize}} \quad & \left[\gamma_A(\mathbf{x}), \gamma_{F_d}(\mathbf{x}), \gamma_t(\mathbf{x})\right], \\ \text{s.t.} \quad & \mathbf{x} \in \mathbf{X} \end{aligned} \tag{28}$$

wherein $\mathbf{x} = \{\mu_t, \mu_{in}, \kappa, \xi\}$ denotes the vector corresponding to undetermined design parameters, and $\mathbf{X}$ represents the feasible domain of design parameters. As described in Eq. (28), the optimization problem is of the multi-objective (MOP) type. Based on the requirement of a comfort-based design method for floor structures, the acceleration response of a

designed structure is expected to be in accordance with the target comfort performance level, which has been preset in advance. To realize such a comfort-based optimization, the $\varepsilon$-constraint approach [52] has been employed, so that the MOP can be transformed into an equivalent single-objective problem (SOP). The weighted average of $\gamma_{F_d}$ and $\gamma_t$ was chosen as the new objective function, and the target value of the floor's acceleration response $\gamma_A$ was considered mathematically as an extra constraint condition in the MOP-to-SOP transformation of a floor structure equipped with TIMS. The new nonlinearly constrained SOP of a floor structure equipped with TIMS can, therefore, be expressed as

$$\begin{aligned} \underset{\mu_t,\mu_{in},\xi,\kappa}{\text{minimize}} \quad & \left[\lambda_{F_d}\gamma_{F_d}\left(\mu_t,\mu_{in},\xi,\kappa\right)+\lambda_{\mu_t}\gamma_t\right], \\ \text{subject to} \quad & \gamma_A\left(\mu_t,\mu_{in},\xi,\kappa\right)=\gamma_{A,\lim} \end{aligned} \tag{29}$$

where $\gamma_{A,\lim}$ denotes the target acceleration response ratio of the floor structure and must be determined in accordance with the desired performance level of the design. Parameters $\lambda_{F_d}$ and $\lambda_{\mu_t}$ denote weight parameters corresponding to $\gamma_{F_d}$ and $\gamma_t$, respectively, which satisfy following constraints.

$$\begin{cases} \lambda_{F_d}+\lambda_{\mu_t}=1 \\ 0\le\lambda_{F_d}\le 1 \\ 0\le\lambda_{\mu_t}\le 1 \end{cases}. \tag{30}$$

The optimal design method also applies to TMD design. If the optimized value of $\mu_{in}$ equals zero, TIMS may degenerate into TMD. A computer program called Optimal Design of TIMS (ODTIMS) has been developed in MATLAB for solving the optimization problem numerically whilst using the proposed technique, whose numerical method can also be found in the references [6, 29].

### 3.3 Design procedure

With reference to the optimal TIMS design equation described in subsection 3.2, the design procedure can be illustrated using the flowchart depicted in Fig. 7, and corresponding TIMS optimization steps can be explained as follow.

Step 1: Perform pre-analysis of the original floor structure to evaluate its initial comfort performance. Based on the preset performance demand and pre-analysis results, determine the target acceleration response ratio $\gamma_{A,\lim}$.

Step 2: Determine weight parameters $\lambda_{F_d}$ and $\lambda_{\mu_t}$ so that influence of the output force and tuned mass can be considered. Substitute $\lambda_{F_d}$, $\lambda_{\mu_t}$, and $\gamma_{A,\lim}$ into Eq. (29), thereby establishing the optimal design equation for TIMS.

Step 3: Solve Eq. (29) to obtain optimized TIMS design parameters— $\mu_t$, $\mu_{in}$, $\kappa$, and $\xi$.

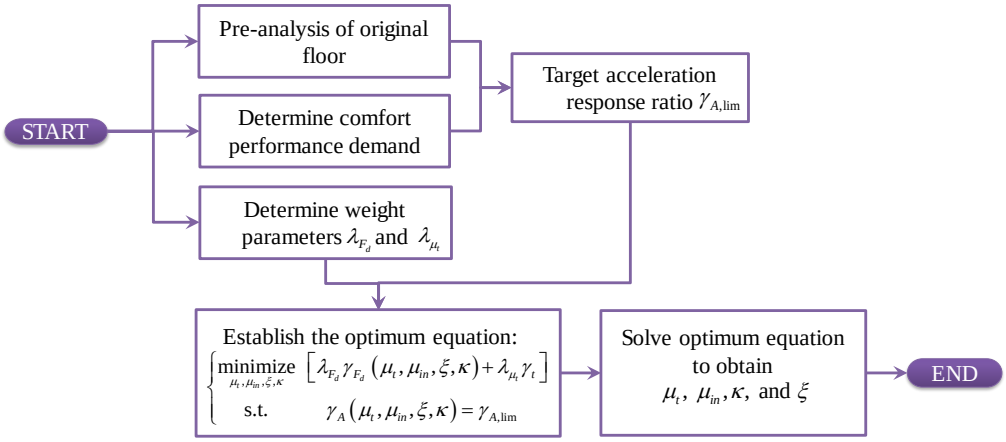


Fig. 7. Flowchart for realizing comfort-based optimal TIMS design.

## 4 Case study

This section describes application of the proposed optimal design method for designing a TIMS based on the target acceleration response level of a floor with minimum control cost. With regard to these design parameters, the vibration mitigation effect of TIMS has been illustrated.

### 4.1 Evaluated acceleration response of TIMS-equipped floor in frequency domain

A series of floor structures similar to those described in Section 3.1 are expected to be equipped with TIMS for acceleration mitigation. The details of target comfort performance levels in design cases were determined and have been listed in Table 1. For each design case, values of $\lambda_{F_d}$ and $\lambda_{\mu_t}$ were determined to be 0.5. Substituting values of $\lambda_{F_d}$, $\lambda_{\mu_t}$, and $\gamma_{A,\lim}$ into Eq. (29), TIMS design parameters were obtained via optimization in MATLAB using ODTIMS. Corresponding values are listed in Table 2.

Table 1. Design cases for floor structure with TIMS.

| Case ID | Case-I-1 | Case-I-2 | Case-I-3 |
|---|---|---|---|
| $\gamma_A$ | 0.65 | 0.50 | 0.25 |

Table 2. TIMS Design parameters for Cases I.

| Case ID | $\mu_{in}$ | $\kappa$ | $\xi$ | $\mu_t$ | $\gamma_{F_d}$ |
|---|---|---|---|---|---|
| Case-I-1 | 0.1887 | 0.1980 | 0.0156 | 0.0934 | 0.0275 |
| Case-I-2 | 0.2409 | 0.2731 | 0.0294 | 0.1307 | 0.0482 |
| Case-I-3 | 0.8840 | 1.4625 | 0.0945 | 0.2805 | 0.0868 |

To illustrate the role of an inerter in TIMS, a comparison was performed between TIMS and TMD, wherein TMD parameters were set to be identical to those of TIMS. Subsequently, values of $H_A(\mathrm{i}\beta\omega)$ and $H_{F_d}(\mathrm{i}\beta\omega)$ corresponding to the floor structure and TIMS and TMD, respectively, were obtained using Eqs. (18) and (19). The power spectral density curve reflects the distribution of the structural response with the walking frequency, which

potentially illustrate the characteristics of acceleration mitigation effects provided by TMD and TIMS. Corresponding curves for $H_A(\mathrm{i}\beta\omega)$ and $H_{F_d}(\mathrm{i}\beta\omega)$ are depicted in Fig. 8 and Fig. 9. As illustrated in Fig. 8, acceleration responses of the floor structure subjected human-induced excitations—within an approximate frequency range of 1.8–2.5 Hz—could be efficiently controlled by TIMS designed using the comfort-based optimal method. Compared to the floor structure equipped with TMD, the maximum acceleration response of floor structure was observed to be suppressed by design TIMS significantly. Meanwhile, the acceleration response can be reduced over a larger frequency bandwidth owing to application of an inerter. Close inspection of Fig. 9 reveals that another significant advantage of using an inerter corresponds to reduction in the TIMS output force, as evaluated by $H_{F_d}(\mathrm{i}\beta\omega)$, in conjunction with satisfaction of the target comfort performance level. Over the given narrow frequency band of human-induced excitations, the TIMS output force was observed to be much lower compared to that observed in the TMD case, thereby demonstrating benefits of the use of an inerter. It can, therefore, be concluded that over the given frequency band, wherein the acceleration mitigation effect of TIMS is greater, the TIMS output force of TIMS is also lower compared to TMD. This comparison illustrates that the inerter plays an important role in reducing the output force of the control device along with satisfaction of the target comfort performance level.

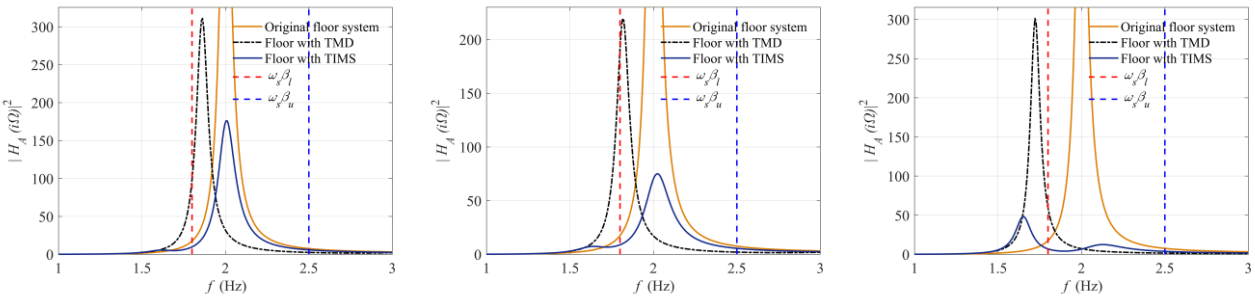


(a) (b) (c)

Fig. 8. Transfer function curves of $H_A(\mathrm{i}\beta\omega_s)$ for floor structure equipped with TIMS and TMD—(a) Case-I-1; (b) Case-I-2; (c) Case-I-3.

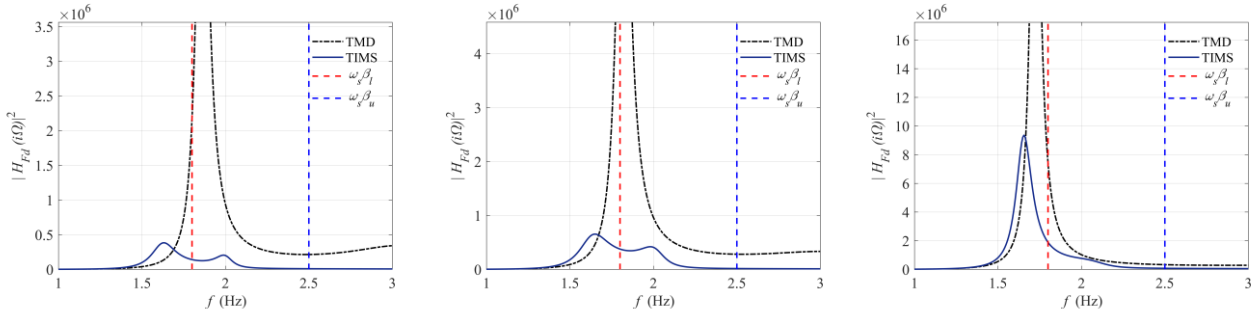


(a) (b) (c)

Fig. 9. Transfer function curves of $H_{F_d}(\mathrm{i}\beta\omega)$ for floor structures equipped with TIMS and TMD—(a) Case-I-1; (b) Case-I-2; (c) Case-I-3.

### 4.2 Comparison study

As discussed above, through use of the proposed optimal design method, the designed TIMS is effective in suppressing the acceleration response of floor structures. The target comfort performance level can be satisfied by the designed TIMS with optimal output force. As mentioned in Section 3.2, the weight of the tuned mass in TIMS can be reduced with the help of the mass enhancement action of the inerter. To realize the tuned mass reduction effect, parametric design of TIMS is a key concern, which has been addressed in the proposed optimal design method.

To illustrate the tuned mass effect of TIMS designed using the proposed method, a comparative analysis of TIMS and TMD was performed, wherein TMD was designed through use of a classical design method for TMD, proposed by Den Hartog [53], wherein the stiffness and nominal damping ratios—$\kappa_{\mathrm{TMD}}$ and $\xi_{\mathrm{TMD}}$, respectively—of TMD are determined based on the given TMD tuned mass ratio $\mu_{t-\mathrm{TMD}}$ in accordance with the following relations.

$$\kappa_{\mathrm{TMD}} = \frac{\mu_{t-\mathrm{TMD}}}{(1+\mu_{t-\mathrm{TMD}})^2},\ \xi_{\mathrm{TMD}} = \frac{\mu_{t-\mathrm{TMD}}}{1+\mu_{t-\mathrm{TMD}}}\sqrt{\frac{3\mu_{t-\mathrm{TMD}}}{8(1+\mu_{t-\mathrm{TMD}})}}. \tag{31}$$

After attainment of the three TMD parameters (i.e., $\kappa_{\mathrm{TMD}}$, $\xi_{\mathrm{TMD}}$, and $\mu_{t-\mathrm{TMD}}$), the acceleration mitigation effect can be calculated using Eq. (23) and evaluated in terms of $\gamma_A$. In this comparative analysis, the authors considered a series of cases, wherein the floor structure considered in Section 4.1 was set to be equipped with TMD and TIMS to satisfy the same comfort performance level. In accordance with the classical TMD design method described in Eq. (31), TMD parameters are mainly dependent on the preset value of $\mu_{t-\mathrm{TMD}}$, which was assumed to be 0.50, 0.25, and 0.10 in this section, a described in Table 3. Table 3 also lists corresponding values of $\gamma_{A-\mathrm{TMD}}$ obtained for the TMDs.

Table 3. Design cases for floor structure with TIMS in Case II.

| Case ID | Case-II-1 | Case-II-2 | Case-II-3 |
|---|---|---|---|
| $\mu_{t-\mathrm{TMD}}$ | 0.50 | 0.25 | 0.10 |
| $\gamma_{A-\mathrm{TMD}}$ | 0.1656 | 0.3154 | 0.7159 |

Under the condition of the same design target in terms of the comfort performance level, values of $\gamma_A$ obtained for the TIMS-equipped floor structure were expected to be identical to those of $\gamma_{A-\mathrm{TMD}}$ listed in Table 3. To take full advantage of the inerter system for reducing the additional TIMS tuned mass, the comfort-based optimal design method was used to obtain TIMS design parameters. Values of weight parameters $\lambda_{F_d}$ and $\lambda_{\mu_t}$ were, respectively, assumed to be 0.0 and 1.0, thereby indicating that the optimal design target of the proposed method was to minimize the TIMS tuned mass along with satisfaction of the desired comfort performance level. Substituting values of $\gamma_A$, $\lambda_{F_d}$, and $\lambda_{\mu_t}$ into Eq. (29), optimal design parameters were obtained by solving the optimal design equation; the said optimized values are listed in Table 4. The factor $\alpha_t = (\mu_t - \mu_{t-\mathrm{TMD}})/\mu_{t-\mathrm{TMD}}$ refers to the tuned mass reduction ratio used to evaluate the effect of TIMS mass reduction. The corresponding value of $\alpha_t$ for each case is also listed in Table 4. Table 4 supports the conclusion that the proposed optimal design method is effective in providing a lightweight device (i.e., designed

TIMS). Compared to the TMD approach for realizing a floor-structure design with the same target comfort performance level, the tuned mass ratio $\mu_t$ of the TIMS was observed reduced by 70.32% (Case-II-1), 53.04% (Case-II-2), and 25.80% (Case-II-3), respectively, when employing the proposed TIMS approach.

Table 4. Design parameters for floor structure equipped with TIMS in Case II.

| Case ID | $\mu_{in}$ | $\kappa$ | $\xi$ | $\mu_t$ | $\mu_{t-\mathrm{TMD}}$ | $\alpha_t$ |
|---|---|---|---|---|---|---|
| Case-II-1 | 0.0236 | 0.2137 | 0.0105 | 0.1484 | 0.50 | -70.32% |
| Case-II-2 | 0.0187 | 0.1352 | 0.0134 | 0.1174 | 0.25 | -53.04% |
| Case-II-3 | 0.0118 | 0.0891 | 0.0087 | 0.0742 | 0.10 | -25.80% |

### 4.3 Time history analysis

Based on optimized TIMS design parameters, this section presents results of time-domain analyses performed to evaluate the effectiveness of the designed TIMS and proposed design method. Governing equations of TIMS- and TMD-equipped floor structures can be solved numerically using the Newmark-$\beta$ method. The thirty human-induce excitations are generated based on Eq. (6) by changing the walking frequency in the limited frequency band, which considered the first three orders of the vertical harmonic loads [48, 49]. The relevant average results of $\gamma_A$ and $\gamma_{F_d}$ were calculated from the time history analysis for the floor under 30 human-induced excitations and listed in Table 5. Expected values of $\gamma_A$ and $\gamma_{F_d}$ listed in Table 5, were obtained from Table 1. As can be realized from Table 5, incorporation of the designed TIMS serves to effectively suppress acceleration responses of the floor. The average acceleration response ratio $\gamma_A$ was observed to closely approximate its value calculated using Eq. (29). As an example, dynamic responses of floor structures with and without incorporation of TIMS in Case-I-3 are depicted in Fig. 10. Inspection of Fig. 10 reveals that acceleration responses of the floor can be simultaneously suppressed by the designed TIMS. During initial states of excitation, use of TIMS demonstrates a significant dynamic response mitigation effect to reduce maximum acceleration responses.

Table 5. Average responses $\gamma_A$ and $\gamma_{F_d}$ of floor structures equipped with TIMS in Cases I and II.

| Case ID | $\gamma_A$ | | $\gamma_{F_d}$ | |
|---|---|---|---|---|
| | Expected value | Average value | Expected value | Average value |
| Case-I-1 | 0.6500 | 0.6520 | 0.0275 | 0.0274 |
| Case-I-2 | 0.5000 | 0.5024 | 0.0482 | 0.0487 |
| Case-I-3 | 0.2500 | 0.2496 | 0.0868 | 0.0845 |

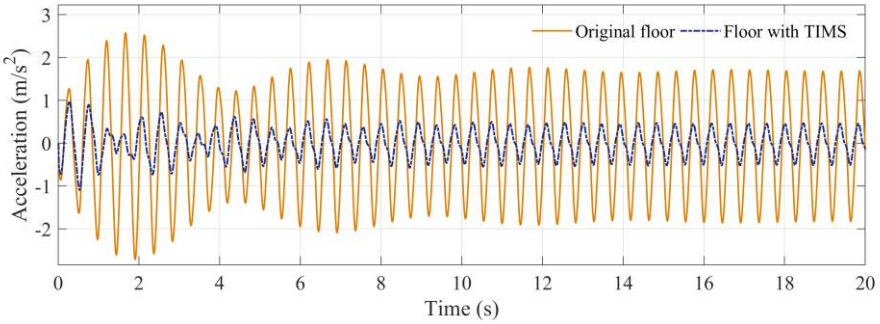


Fig. 10. Acceleration response comparison between original and TIMS-equipped floor structures in Cases-I-3 ( $f$ =2.2 Hz).

As regards Case-II-2, acceleration responses of the TIMS- and TMD-equipped floor structures in the same time domain are depicted in Fig. 11. Across the entire time domain, acceleration response of the TIMS-equipped floor structure was found to be in line with that of the TMD-equipped floor structure with high accuracy. The RMS value of the acceleration response of the TIMS-equipped floor (represented by the blue horizontal line in Fig. 11, 0.71 $m/s^2$) nearly coincides with that of the TMD-equipped floor (represented by the red horizontal line in Fig. 11, 0.70 $m/s^2$). In addition, the maximum acceleration of the TIMS-equipped floor (1.17 $m/s^2$) is lightly larger than that of the TMD-equipped floor (1.02 $m/s^2$), which is not closely related to the comfort-based issue of the floor structures. The designed TIMS was, therefore, found to be effective as a light device capable of achieving the desired comfort performance level of the floor. Compared to the traditional TMD technique used to obtain the same comfort performance level, the value of $\mu_t$ corresponding to TIMS can be reduced so that its application can be extended by reducing the actual mass of the system, which can be installed more flexibly within a structure.

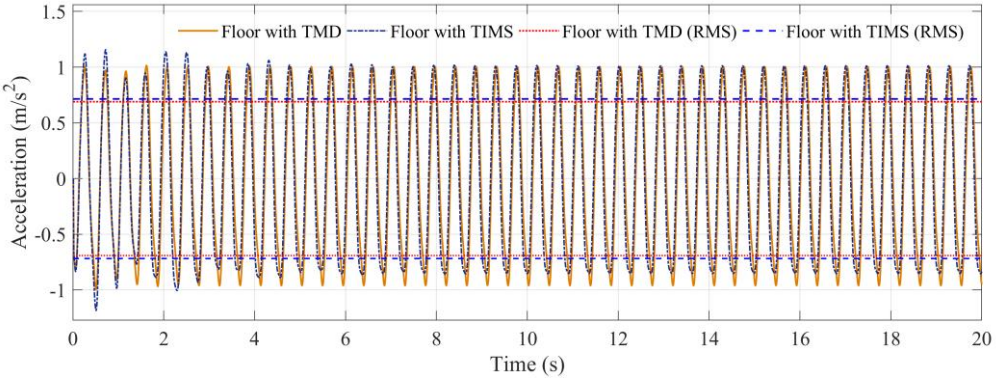


Fig. 11. Acceleration response comparison between TMD- and TIMS-equipped floor structures in Case-II-2 ( $f$ =2.2 Hz).

## 5 Conclusions

This study describes development of a comfort-based optimal design method for TIMS-equipped floor structures to reduce their vertical vibration response when subjected to human-induced excitations. Based on the theory of random vibration analysis, expressions for optimization indicators of the TIMS design method have been deduced. Subsequently,

the proposed optimal design method was employed to obtain TIMS parameters. A series of design cases have been established and investigated under different comfort performance levels desired to be achieved by the floor structure. TIMS-equipped floor structures corresponding to each design case have been designed and examined via time-domain analysis, based on the results of which following conclusions have been drawn.

(1) Using the proposed comfort-based optimal design method, the resulting TIMS-equipped floor structure provides effective results with regard to acceleration mitigation with optimal output force and additional TIMS tuned mass. Use of the proposed technique provides a balance between the floor's acceleration response, vibration control costs, and tuned mass.

(2) Compared to the traditional TMD, acceleration responses of the floor can be more effectively reduced through use of the TIMS with the same tuned mass. This implies that a higher comfort performance can be obtained using the TIMS inerter element.

(3) Nearly identical comfort performances can be realized using TIMS- and TMD-equipped floor; however, tuned mass of the proposed TIMS is considerably smaller compared to that of the traditional TMD method. The mass enhancement effect of the inerter element can be fully utilized when employing the proposed comfort-based design approach.

(4) Considering the lower additional tuned mass, applications of the TIMS technique can be extended and its installation made more flexible. The corresponding experiment study needs to be conducted in the near future.

**Funding:** This study was supported by the Shanghai Pujiang Program [Grant number: 17PJ1409200], the National Natural Science Foundation of China [Grant number: 51778489], the Fundamental Research Funds for the Central Universities [Grant number: 22120180064], and the Key Laboratory of Green Building in West China under [Grant number: LSKF201804].

**References**

[1] G.W. Housner, L.A. Bergman, T.K. Caughey, A.G. Chassiakos, R.O. Claus, S.F. Masri, R.E. Skelton, T.T. Soong, B.F. Spencer, J.T.P. Yao, Structural control: Past, present, and future, Journal of Engineering Mechanics-ASCE 123(9) (1997) 897-971. http://dx.doi.org/10.1061/(Asce)0733-9399(1997)123:9(897).

[2] L. Zhang, M. Su, C. Zhang, h. Shen, M.M. Islama, R.F. Zhang, A design method of viscoelastic damper parameters based on the elastic-plastic response reduction curve, Soil Dynamics and Earthquake Engineering 117(2019) 149-163.

[3] R.F. Zhang, C. Wang, C. Pan, H. Shen, Q. Ge, L. Zhang, Simplified design of elastoplastic structures with metallic yielding dampers based on the concept of uniform damping ratio, Engineering Structures 176(2018) 734-745.

[4] E. Shahabpoor, A. Pavic, V. Racic, Structural vibration serviceability: New design framework featuring human-structure interaction, Engineering Structures 136(2017) 295-311. https://doi.org/10.1016/j.engstruct.2017.01.030.

[5] H. Shen, R.F. Zhang, D.G. Weng, C. Gao, H. Luo, C. Pan, Simple design method of structure with metallic yielding dampers based on elastic–plastic response reduction curve, Engineering Structures 150(2017) 98-114.

http://dx.doi.org/10.1016/j.engstruct.2017.07.047.

[6] C. Pan, R.F. Zhang, Design of structure with inerter system based on stochastic response mitigation ratio, Structural Control & Health Monitoring 25(6) (2018) e2169. http://dx.doi.org/10.1002/stc.2169.

[7] L.F. Hao, R.F. Zhang, K. Jin, Direct design method based on seismic capacity redundancy for structures with metal yielding dampers, Earthquake Engineering & Structural Dynamics 47(2) (2018) 515-534. https://doi.org/10.1002/eqe.2977.

[8] M.L. Chang, C.C. Lin, J.M. Ueng, K.H. Hsieh, J.F. Wang, Experimental study on adjustable tuned mass damper to reduce floor vibration due to machinery, Structural Control & Health Monitoring 17(5) (2010) 532-548. https://doi.org/10.1002/stc.330.

[9] L.F. Costa-Neves, J.G.S.D. Silva, L.R.O.D. Lima, S. Jordão, Multi-storey, multi-bay buildings with composite steel-deck floors under human-induced loads: The human comfort issue, Computers & Structures 136(3) (2014) 34-46. https://doi.org/10.1016/j.compstruc.2014.01.027.

[10] T. Ji, B.R. Ellis, Floor vibration induced by dance-type loads: Verification, The Structural Engineer 72(1994) 45-50.

[11] M. Setareh, J.K. Ritchey, T.M. Murray, J.H. Koo, M. Ahmadian, Semiactive tuned mass damper for floor vibration control, Journal Structural Engineering 133(2) (2007) 242-250. https://doi.org/10.1016/j.soildyn.2016.08.037.

[12] I.M. Díaz, P. Reynolds, Acceleration feedback control of human-induced floor vibrations, Engineering Structures 32(1) (2010) 163-173. https://doi.org/10.1016/j.engstruct.2009.09.003.

[13] F. Venuti, L. Bruno, Mitigation of human-induced lateral vibrations on footbridges through walkway shaping, Engineering Structures 56(6) (2013) 95-104. https://doi.org/10.1016/j.engstruct.2013.04.019.

[14] H. Kida, Y. Watanabe, S. Nakaminami, H. Tanaka, Y. Sugimura, K. Saito, K. Ikago, N. Inoue, Full-scale dynamic tests of tuned viscous mass damper with force restriction mechanism and its analytical verification, Journal of Structural & Construction Engineering 76(665) (2011) 1271-1280.

[15] F. Tubino, G. Piccardo, Tuned Mass Damper optimization for the mitigation of human-induced vibrations of pedestrian bridges, Meccanica 50(3) (2015) 809-824. https://doi.org/10.1007/s11012-014-0021-z.

[16] M. Carlos, An alternative methodology for designing tuned mass dampers to reduce seismic vibrations in building structures, Earthquake Engineering & Structural Dynamics 41(14) (2012) 2059-2073. https://doi.org/10.1002/eqe.2174.

[17] C.Á. Caetano E, Moutinho C, Magalhães F, Studies for controlling human-induced vibration of the Pedro e Inês footbridge, Portugal. Part 2: Implementation of tuned mass dampers, Engineering Structures 32(2010) 1082-1091. https://doi.org/10.1016/j.engstruct.2009.12.033.

[18] K. Lievens, G. Lombaert, G.D. Roeck, P.V.D. Broeck, Robust design of a TMD for the vibration serviceability of a footbridge, Engineering Structures 123(2016) 408-418. https://doi.org/10.1016/j.engstruct.2016.05.028.

[19] Y. Hu, M.Z.Q. Chen, Y. Sun, Comfort-oriented vehicle suspension design with skyhook inerter configuration, Journal of Sound & Vibration 405(2017) 34-47. https://doi.org/10.1016/j.jsv.2017.05.036.

[20] Y. Hu, M.Z.Q. Chen, Performance evaluation for inerter-based dynamic vibration absorbers, International Journal of Mechanical Sciences 99(2015) 297-307. https://doi.org/10.1016/j.ijmecsci.2015.06.003.

[21] Q.J. Chen, Z.P. Zhao, R.F. Zhang, C. Pan, Impact of soil–structure interaction on structures with inerter system, Journal of Sound & Vibration 433(2018) 1-15. https://doi.org/10.1016/j.jsv.2018.07.008.

[22] T. Arakaki, H. Kuroda, F. Arima, Y. Inoue, K. Baba, Development of seismic devices applied to ball screw : Part 1 Basic performance test of RD-series, Journal of Architecture and Building Science 8(1999) 239-244.

[23] M.C. Smith, Synthesis of mechanical networks: The inerter. Automatic Control, IEEE Transactions 47(10) (2002) 1648-1662.

[24] M.C. Smith, Force-controlling mechanical device, in, Cambridge University Technical Services, Ltd. (Cambridge,

GB), 2008.

[25] C. Papageorgiou, N.E. Houghton, M.C. Smith, Experimental testing and analysis of inerter devices, Journal of Dynamic Systems, Measurement, and Control 131(1) (2008) 101-116. http://dx.doi.org/10.1115/1.3023120.

[26] A. Gonzalez-Buelga, L.R. Clare, S.A. Neild, J.Z. Jiang, D.J. Inman, An electromagnetic inerter-based vibration suppression device, Smart Materials and Structures 24(5) (2015) 055-015. https://doi.org/10.1088/0964-1726/24/5/055015.

[27] M.C. Smith, N.E. Houghton, P.J.G. Long, A.R. Glover, Force-controlling hydraulic device, in, Cambridge Enterprise Limited (Cambridge, GB), 2011.

[28] K. Ikago, K. Saito, N. Inoue, Seismic control of single-degree-of-freedom structure using tuned viscous mass damper, Earthquake Engineering & Structural Dynamics 41(3) (2012) 453-474. https://doi.org/10.1002/eqe.1138.

[29] C. Pan, R.F. Zhang, C. Li, H. Luo, H. Shen, Demand-based optimal design of oscillator with parallel-layout viscous inerter damper, Structural Control & Health Monitoring 25(1) (2018) e2051. http://dx.doi.org/10.1002/stc.2051.

[30] R.F. Zhang, Z.P. Zhao, C. Pan, Influence of mechanical layout of inerter systems on seismic mitigation of storage tanks, Soil Dynamics and Earthquake Engineering 114(2018) 639-649. https://doi.org/10.1016/j.soildyn.2018.07.036.

[31] R.F. Zhang, Z.P. Zhao, K. Dai, Seismic response mitigation of a wind turbine tower using a tuned parallel inerter mass system, Engineering Structures 180(2019) 29-39. https://doi.org/10.1016/j.engstruct.2018.11.020.

[32] D. De Domenico, G. Ricciardi, Improving the dynamic performance of base-isolated structures via tuned mass damper and inerter devices: A comparative study, Structural Control and Health Monitoring 25(10) (2018) e2234. https://doi.org/10.1002/stc.2234.

[33] Y. Nakamura, A. Fukukita, K. Tamura, I. Yamazaki, T. Matsuoka, K. Hiramoto, K. Sunakoda, Seismic response control using electromagnetic inertial mass dampers, Earthquake Engineering & Structural Dynamics 43(4) (2014) 507-527. http://dx.doi.org/10.1002/eqe.2355.

[34] F.C. Wang, C.W. Chen, M.K. Liao, M.F. Hong, Performance analyses of building suspension control with inerters, in: Decision and Control, 2007 IEEE Conference on, 2007, pp. 3786-3791.

[35] I.F. Lazar, D.J. Wagg, S.A. Neild, An inerter vibration isolation system for the control of seismically excited structures, in: International Conference on Urban Earthquake Engineering, Tokyo, Japan, 2013.

[36] H. Luo, R.F. Zhang, D.G. Weng, Mitigation of liquid sloshing in storage tanks by using a hybrid control method, Soil Dynamics & Earthquake Engineering 90(2016) 183-195. https://doi.org/10.1016/j.soildyn.2016.08.037.

[37] L. Marian, A. Giaralis, Optimal design of a novel tuned mass-damper–inerter (TMDI) passive vibration control configuration for stochastically support-excited structural systems, Probabilistic Engineering Mechanics 38(2014) 156-164. https://doi.org/10.1016/j.probengmech.2014.03.007.

[38] D. De Domenico, G. Ricciardi, An enhanced base isolation system equipped with optimal tuned mass damper inerter (TMDI), Earthquake Engineering & Structural Dynamics 47(5) (2018) 1169-1192. https://doi.org/10.1002/eqe.3011.

[39] D. De Domenico, N. Impollonia, G. Ricciardi, Soil-dependent optimum design of a new passive vibration control system combining seismic base isolation with tuned inerter damper, Soil Dynamics and Earthquake Engineering 105(2018) 37-53. https://doi.org/10.1016/j.soildyn.2017.11.023.

[40] D. De Domenico, G. Ricciardi, Optimal design and seismic performance of tuned mass damper inerter (TMDI) for structures with nonlinear base isolation systems, Earthquake Engineering and Structural Dynamics 47(12) (2018) 2539-2560. https://doi.org/doi:10.1002/eqe.3098.

[41] T. Hashimoto, K. Fujita, M. Tsuji, I. Takewaki, Innovative base-isolated building with large mass-ratio TMD at basement for greater earthquake resilience, Future Cities and Environment 1(1) (2015) 9. ://doi.org/10.1186/s40984-015-0007-6.

[42] D. Pietrosanti, M.D. Angelis, M. Basili, Optimal design and performance evaluation of systems with Tuned Mass Damper Inerter (TMDI), Earthquake Engineering & Structural Dynamics 46(8) (2017) 1367 - 1388. https://doi.org/10.1002/eqe.2861.

[43] P. Brzeski, T. Kapitaniak, P. Perlikowski, Novel type of tuned mass damper with inerter which enables changes of inertance, Journal of Sound & Vibration 349(2015) 56-66. https://doi.org/10.1016/j.jsv.2015.03.035.

[44] P. Brzeski, M. Lazarek, P. Perlikowski, Experimental study of the novel tuned mass damper with inerter which enables changes of inertance, Journal of Sound & Vibration 404(2017) 47-57. http://dx.doi.org/10.1016/j.jsv.2017.05.034.

[45] N. Poovarodom, S. Kanchanosot, P. Warnitchai, Application of non-linear multiple tuned mass dampers to suppress man-induced vibrations of a pedestrian bridge, Earthquake Engineering & Structural Dynamics 32(7) (2003) 1117-1131. https://doi.org/10.1002/eqe.265.

[46] A.K. Chopra, Dynamics of structures: Theory and applications to earthquake engineering, forth edition, Prentice Hall, NJ, USA, 2012.

[47] L. Marcheggiani, S. Lenci, On a model for the pedestrians-induced lateral vibrations of footbridges, Meccanica 45(4) (2010) 531-551.

[48] S. Živanović, A. Pavic, P. Reynolds, Vibration serviceability of footbridges under human-induced excitation: a literature review, Journal of Sound & Vibration 279(1–2) (2005) 1-74. https://doi.org/10.1016/j.jsv.2004.01.019.

[49] H. Bachmann, W. Ammann, Vibrations in structures induced by man and machines, Canadian Journal of Civil Engineering 15(6) (1987) 1086-1087.

[50] X. Chen, Y. Ding, Z. Zhang, P. Sun, A. Li, Investigations on serviceability control of long-span structures under human-induced excitation, Earthquake Engineering & Engineering Vibration 11(1) (2012) 57-71. http://dx.doi.org/10.1007/s11803-012-0098-0.

[51] G. Piccardo, F. Tubino, Equivalent spectral model and maximum dynamic response for the serviceability analysis of footbridges, Engineering Structures 40(2012) 445-456. https://doi.org/10.1016/j.engstruct.2012.03.005.

[52] V. Chankong, Y. Haimes, Multiobjective decision making theory and methodology, Elsevier, New York, 1983.

[53] J.P. Den Hartog, Mechanical vibrations, forth edition, McGraw-Hill, Dover, New York, USA, 1956.